IEEE Access
Multidisciplinary | Rapid Review | Open Access Journal

Received November 10, 2019, accepted December 2, 2019, date of publication December 30, 2019, date of current version January 8, 2020.

Digital Object Identifier 10.1109/ACCESS.2019.2962963

2.5-D Inversion of Advanced Detection Transient Electromagnetic Method in Full Space

JIULONG CHENG[1], JUNJIE XUE[1], JIN ZHOU[2], YI DONG[1], AND LAIFU WEN[3]

[1]State Key Laboratory of Coal Resources and Safe Mining, China University of Mining and Technology, Beijing 100083, China
[2]China Railway Eryuan Engineering Group Company Ltd., Chengdu 610031, China
[3]Department of Earth Science and Engineering, Hebei University of Engineering, Handan 056009, China

Corresponding author: Jiulong Cheng (jlcheng@126.com)

This work was supported in part by the National Natural Science Foundation of China under Grant 41974088 and Grant 51574250, and in part by the National Key Research and Development Program of China under Grant 2017YFC0804105.

ABSTRACT The transient electromagnetic method (TEM) can be applied in detecting coal mining heading face with multiple angles. However, a 1-D inversion scheme cannot fit this kind of multi-angle data-receiving system well, nor reducing detection accuracy. Developing a 2.5-D inversion method is necessary for TEM multi-angle data. The expressions of the vertical and horizontal magnetic dipole source at any position in the layered medium are derived on the basis of the potential function and the boundary conditions of the electromagnetic field. Then, the electromagnetic field of the magnetic dipole source with multiple angles can be obtained through vector stacking. A low-resistance anomalous body above the roof in front of a roadway excavation was identified by applying a 2.5-D least square inversion method in mine TEM-advanced detection to verify the effectiveness of the inversion method. Moreover, the method was used to detect water inrush from one side of the roadway in a coal mine in Shandong Province, China. Furthermore, the inversion results were verified by the information of boreholes and excavation. The proposed 2.5-D inversion method has a higher interpretation accuracy and resolution than the 1-D inversion method of the model and the measured data.

INDEX TERMS Mine transient electromagnetic method, advanced detection, arbitrary angle field source, 2.5-dimensional inversion, damped least squares method.

I. INTRODUCTION

The condition of coal seams has become complicated with the increase in coal mining depths in China. Mine water inrush poses a serious threat to the safety of coal mines in recent years [1]–[3]. At present, the main geophysical prospecting methods used in mine water disaster detection include direct current methods, mine transient electromagnetic method (TEM), ground-penetrating radar, electromagnetic wave perspective, and infrared temperature method [4].

TEM is widely used for detecting coal water-bearing structures on ground [5], [6]. However, its detection accuracy cannot meet the requirements of coal mine production safety. Mine TEM, which is applied in underground coal mine's working face with strong penetration through high-resistivity bodies, is sensitive to low-resistivity bodies [7]. Regarding the small spaces, the multi-turn small loop-transmitting and -receiving device for mine TEM was applied to the detection of roadway and water-bearing structures in the roof and floor, which plays an important role in coal mine flood damage control. Mine TEM cannot apply the theory of traditional ground TEM directly because it collects data in underground full space. Moreover, the collected data are disturbed by metallic materials, cables, and other facilities in the roadway, which increase the difficulty of inversion [8].

Currently, 1-D inversion, which uses a linear or approximate inversion method from a single point, is the main method used for processing and interpreting mine TEM. The 1-D inversion results, which cannot show the prolife of geological information accurately, are usually combined point-by-point to form a pseudo 2D section [9]. Thus, applying 2.5-D inversion method in actual conditions is necessary [10].

The 2.5-D approach has been widely investigated by applying 3-D field sources and 2-D methods to actual geological conditions [2], [11]. Xiong (2004) proposed a method for calculating the sensitivity matrix by integrating the dot product of auxiliary and original electromagnetic fields in 2.5-D TEM inversion [12]. Schaa (2010) proposed a fast and approximate 3-D inversion method for TEM data [13]. Chen (2018) applied a nonlinear conjugate gradient (NLCG) method to

The associate editor coordinating the review of this manuscript and approving it for publication was Giovanni Angiulli.

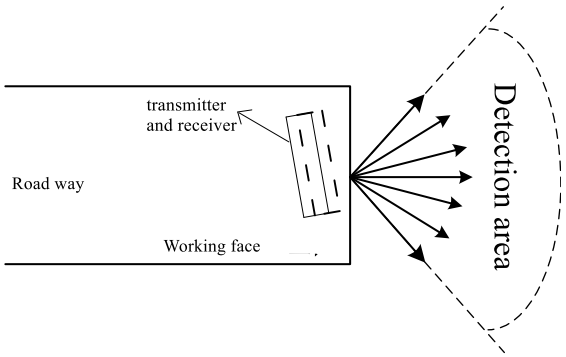

FIGURE 1. Mine TEM advanced detection with multiple angles.

inversion in the field of natural gas hydrate detection through controlled source electromagnetic detection, whose results were basically consistent with seismic reflection and logging results [14]. Li (2009) proposed a Gauss–Newton method for 2.5-D cross-well electromagnetic inversion, which is based on the finite-different time-domain (FDTD) by YEE [15].

Regarding ground TEM approach, the 2.5-D airborne TEM inversion method has been widely studied recently. Wilson (2006) proposed a method for 2.5-D airborne TEM inversion using a 2-D finite element method combined with a 3-D emission source [16]. Furthermore, Kirkegaard (2015) proposed a parallel inversion method to accelerate the computation speed [17]. Li (2016) proposed a 2.5-D airborne TEM inversion method in the frequency domain based on the singular value decomposition and least squares methods [18]. Qiang (2016) proposed a 2.5-D airborne TEM inversion method by NLCG and obtained good results [19].

However, the literature that focus on 2.5-D mine TEM advanced detection with a multi-turn small loop source was limited. In this paper, to obtain a high-resolution inversion result with multi-angle in-mine TEM, we first use a nonlinear inversion method to obtain a 1-D result, which is used as the initial model for the 2.5-D inversion. Subsequently, the 2.5-D mine TEM advanced detection can be realized through a least squares approach by a vector stacking method to determine the electromagnetic values of multiple angles. Finally, we apply the proposed method to modeling and actual measurement to verify its accuracy and reliability.

II. 1-D TEM ADVANCED DETECTION IN FULL SPACE

Mine TEM prospecting is carried out in underground roadways using a multi-turn detection loop device. Given the small coil, the distance among points is compact (generally 2–20 m), which can reduce the volume effect and improve the lateral resolution of exploration. Nearness to the target body can improve the induction signal intensity of the abnormal body. A diagram of mine TEM-advanced detection with multiple angles is shown in Figure 1. The normal direction is observed along the horizon, and some measuring points are arranged on the side of the coil.

Taking the vertical component of magnetic field H_z as an example, the vector potential function $\tilde{A}_{z,i}$ satisfies the Helmholtz equation with an emission source and can be expressed as follows [20]:

$$\tilde{A}_{z,i} = c_i e^{-u_i(z_{i+1}-z)} + d_i e^{-u_i(z-z_i)} - \frac{u_i}{\lambda^2}\left(a_i e^{-u_i(z_{i+1}-z)} - b_i e^{-u_i(z_{i+1}-z)}\right), \quad (1)$$

where $u_i = \sqrt{\lambda^2 - k_i^2}$; z_i represents the interface depth of the i^{th} layer; and a_i, b_i, c_i, and d_i represent the coefficients of the source, which are derived by the recurrence formula.

$$H_z^{KMD} = -\frac{1}{z}\frac{My}{2\pi r}\int_0^\infty \left\{\lambda^2\left(c_i e^{u_i(z-z_{i+1})} + d_i e^{-u_i(z-z_i)}\right) \pm \frac{1}{2}\delta_{ij} e^{-u_j|z-z_i|}\right\}_1 (\lambda r)\lambda^2 d\lambda, \quad (2)$$

$$H_z^{VMD} = \frac{My}{2\pi}\int_0^\infty \left[p_i e^{u_i(z-z_{i+1})} + q_i e^{-u_i(z-z_i)}\right] J_0(\lambda r)\lambda^3 d\lambda, \quad (3)$$

where $M = I\pi r^2$, which represents the magnetic moment; $p_i = \frac{2MJ_1(\lambda a)}{\lambda a}c_i$; $q_i = \frac{2MJ_1(\lambda a)}{\lambda a}d_i$; J_1 and J_0 represent the 1^{st} and 0^{th} Bessel functions, respectively. H is the electromagnetic value; *HMD* and *VMD* represent the horizontal and the vertical magnetic dipole sources, respectively;r, δ, and $\hat{z}$ represent the coil radius, the Dirac function, and the impedance, respectively. Similarly, other components of the electromagnetic field can be calculated.

Using the Hankel transform on (2), (3) can be expressed as follows:

$$rH_z^{HMD} = -\frac{1}{\hat{z}}\frac{My}{2\pi r}\sum_{k=1}^{n} W_k^1(\lambda^2(c_i e^{-u_i(z-z_{i+1})} + d_i e^{-u_i(z-z_i)}) \pm \frac{1}{2}\delta_{ij} e^{-u_j|z-z_i|})\lambda_k^2, \quad (4)$$

$$rH_z^{VMD} = \frac{My}{2\pi}\sum_{k=1}^{n} W_k^2\left[p_i e^{u_i(z-z_{i+1})} + q_i e^{-u_i(z-z_i)}\right]\lambda_k^3, \quad (5)$$

$$\lambda_k = \frac{1}{r}\times 10^{q+(k-1)s}, \quad k = 1, 2....n, \quad (6)$$

where q and s represent the correlation coefficients that are used in calculating wavelength λ_k, and W_k^1 and W_k^2 denote the filter coefficients. In this paper, we use the Guptasarma 120- and 140-point filter coefficients to calculate the 0^{th} and 1^{st} Bessel functions, respectively. Then, the electromagnetic values can be obtained in the time domain based on the cosine polygonal line approximations of the inverse Fourier transforms.

III. INVERSION OF 1-D SIMULATED ANNEALING-PARTICLE SWARM OPTIMIZATION

Particle swarm optimization (PSO) is a kind of stochastic evolution optimization algorithm that expresses the solution of a preparative optimization problem as the location of multiple particles in a search space. This algorithm evaluates the particles using the objective function value of the particle position and selects the location of the optimal particle as

the solution to the problem. The iterative formula can be expressed as follows [21]:

$$v_{i,j}^{k+1} = v_{i,j}^{k} + c_1 \cdot r_1 \cdot (pbest\,\rho_{i,j}^{k} - \rho_{i,j}^{k}) + c_2 \cdot r_2 \cdot (gbest\,\rho_{i,j}^{k} - \rho_{i,j}^{k}) \quad (7)$$

$$\rho_{i,j}^{k+1} = \rho_{i,j}^{k} + \rho_{i,j}^{k+1}, \quad (8)$$

where v denotes speed, c_1 and c_2 denote learning factors, r_1 and r_2 are two random numbers with uniform distribution within (0, 1), $\rho_{i,j}^{k}$ represents the value of an individual particle at the k^{th} iteration, *pbestx* denotes the individual extremum, *gbestx* denotes the population extremum, i denotes the particle, and j denotes the dimension of the search space. Although the PSO algorithm requires to set only a small number of parameters and converges rapidly, it is easily trapped in the local minima. The simulated annealing (SA) method can then be applied to improve the inversion accuracy.

The SA-PSO algorithm considers the PSO algorithm as the main process and applies the SA mechanism. The Metropolis criterion can control the updating process of the particle's position and velocity. Moreover, this criterion accepts the poor adaptable solution with a certain probability to make particles avoid local extrema and premature termination of the algorithm. Particles gradually converge to the global optimal solution when the annealing temperature is adjusted in the criterion, which is expressed in (9). The Metropolis criterion can be expressed as follows [22]:

$$p_{ij}(T) = \begin{cases} 1, & \rho_{i,j}^{k+1} \le \rho_{i,j}^{k} \\ \exp\dfrac{\rho_{i,j}^{k+1} - \rho_{i,j}^{k}}{T}, & \rho_{i,j}^{k+1} > \rho_{i,j}^{k}, \end{cases} \quad (9)$$

where $T(k) = T_0/(1 + \beta n)$; T_0 denotes initial speed; β is a small constant, which is selected to be 0.1 in this paper; and n is the number of current iterations.

The specific iteration steps are presented as follows:

(1) Use beta distribution to initialize the position, velocity, and annealing temperature of particles.

(2) Update the position and velocity of particles according to (7) and (8).

(3) Use the updated particle to calculate H_z, then update the individual and all optimal values of particles.

(4) Determine whether to accept the new solution according to the Metropolis criterion.

(5) Determine whether the iteration termination condition is satisfied.

IV. 2.5-D MINE TEM METHOD

A. 2.5-D FORWARD CALCULATION

Without considering displacement current, the Maxwell equations of electromagnetic file can be expressed as

$$\nabla \times E(r,t) = -\frac{\partial B(r,t)}{\partial t} + j_m(r,t), \quad (10)$$

$$\nabla \times H(r,t) = j(r,t), \quad (11)$$

$$B(r,t) = \mu(r)H(r,t), \quad (12)$$

$$j(r,t) = \sigma(r)E(r,t), \quad (13)$$

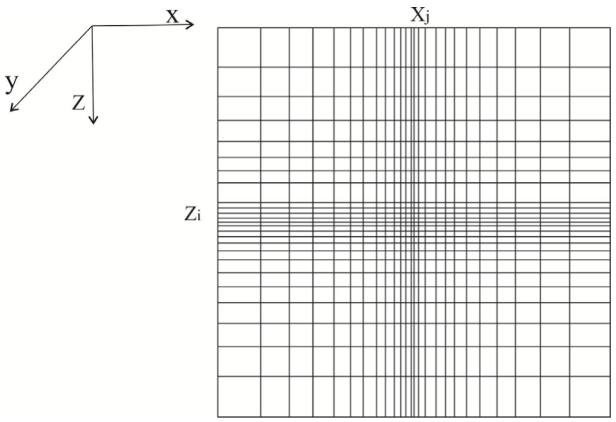

FIGURE 2. Full space finite difference time domain grid.

here $E(r,t)$, $H(r,t)$, $B(r,t)$, $j_m(r,t)$, $j(r,t)$, $\sigma(r)$, and $\mu(r)$ enote electric intensity, magnetic intensity, magnetic induction intensity, magnetic flux density, electric current density, conductivity, and permeability, respectively. The diffusion equation of the secondary field can be calculated by taking curl on both sides of formula (11), substituting formula (10), and then ignoring the primary field and turn-off effect; thereby expressed as follows:

$$\nabla^2 H(r,t) = \sigma(r)\mu(r)\frac{\partial H(r,t)}{\partial t}. \quad (14)$$

Integrating (14) in ΔV gives

$$\iiint_{\Delta V} \frac{\partial^2 H}{\partial x^2} + \frac{\partial^2 H}{\partial y^2} + \frac{\partial^2 H}{\partial z^2} = \iiint_{\Delta V} \sigma(r)\mu(r)\frac{\partial H(r,t)}{\partial t}. \quad (15)$$

The difference approximation of (15) is computationally heavy. This issue is avoided by using Fourier transform (16) in 2.5-D space:

$$\tilde{H}(x,y,z) = \int_{-\infty}^{+\infty} H(x,y,z)e^{-i\lambda y}dy, \quad (16)$$

$$\iiint_{\Delta V} \frac{\partial^2 \tilde{H}}{\partial x^2} - \lambda^2 \tilde{H} + \frac{\partial^2 \tilde{H}}{\partial z^2} = \iiint_{\Delta V} \sigma(r)\mu(r)\frac{\partial \tilde{H}(r,t)}{\partial t}. \quad (17)$$

The original electromagnetic field can be transformed in the wave domain by the Dufort–Frankel difference approach: (18) and (19), as shown at the top of the next page, where $\mu, \bar{\sigma}$, and Δ represent magnetic permeability, average conductivity, and step size, respectively.

The forward model is divided into several small rectangular elements (Figure 2) by a nonuniform grid to improve the accuracy and efficiency of the electromagnetic field. The grid lines are denser near the source where the minimum grid size is 2 m × 2 m, and the spacing increases by a linear expansion factor of 1.1 for each step outward. The magnetic field in the node can be expressed as

$$H_{i,j}^{\prime n+1} = \frac{4\Delta t}{\mu\bar{\sigma}_{i,j} - 2\Delta t A_5}(A_1 H_{i-1,j}^{\prime n} + A_2 H_{i+1,j}^{\prime n} + A_3 H_{i,j-1}^{\prime n} + A_4 H_{i,j+1}^{\prime n}) + \frac{\mu\bar{\sigma}_{i,j} + 2\Delta t A_5}{\mu\bar{\sigma}_{i,j} - 2\Delta t A_5} H_{i,j}^{\prime n-1}, \quad (20)$$

$$\frac{\partial H'^{n}_{i,j}}{\partial t} = \frac{H'^{n+1}_{i,j} - H'^{n-1}_{i,j}}{2\Delta t}, \tag{18}$$

$$\frac{H'^{n+1}_{i,j} - H'^{n-1}_{i,j}}{2\Delta t} = \frac{H'^{n}_{i-1,j} + H'^{n}_{i+1,j} + H'^{n}_{i,j-1} + H'^{n}_{i,j+1} - \frac{1}{2}(4 + \Delta^2\lambda^2)(H'^{n+1}_{i,j} + H'^{n-1}_{i,j})}{\mu\bar{\sigma}_{i,j}\Delta^2}, \tag{19}$$

where $A_1 = \frac{1}{\Delta z_{i-1}(\Delta z_{i-1}+\Delta z_i)}$, $A_2 = \frac{1}{\Delta z_i(\Delta z_{i-1}+\Delta z_i)}$, $A_3 = \frac{1}{\Delta x_{j-1}(\Delta x_{j-1}+\Delta x_j)}$, $A_4 = \frac{1}{\Delta x_j(\Delta x_{j-1}+\Delta x_j)}$, and $A_5 = -\left(\frac{1}{\Delta z_i \Delta z_{i+1}} + \frac{1}{\Delta x_j \Delta x_{j+1}} + \frac{\lambda^2}{2}\right)$.

The magnetic field value $H^n_{i,j}$ is expressed as the average value of the forward and backward difference calculation. The magnetic field value within the grid can be calculated separately in an iterative process. The concrete steps are presented as follows: Calculate the magnetic values $H^{n-1}_{i,j}$ and $H^{n+1}_{i,j}$ when time step $(n+1)\Delta t$ is odd, and calculate the electromagnetic values $H^n_{i,j}$ and the $H^{n+2}_{i,j}$ when time step $(n+2)\Delta t$ is even. The magnetic values in the grid can be obtained by repeating the process mentioned above. Set up the time step as one half of the time of which the electromagnetic wave propagates a space step, and the original time step is 1.2×10^{-7}s. After obtaining the magnetic values in the wave domain, the values can be transformed into the space domain by exponential fitting. Setting up the boundary absorption conditions is necessary to simulate infinite space. In the paper, we use the second-order boundary absorption condition [7].

B. RESPONSE OF ELECTROMAGNETIC FIELD IN ANY DIRECTION

Changing the normal direction of the mine TEM multi-turn small coil can provide electromagnetic response from any direction. While the normal direction of the coil has a certain angle with the rock interface, the corresponding electromagnetic field value needs to be initialized to the source. The expressions of the vertical and horizontal magnetic dipole source at any position in the layered medium can be derived based on the potential function and boundary conditions of the electromagnetic field. Then, the electromagnetic values can be calculated in any direction by vector stacking.

In mine TEM, the multi-turn small coil is used as an emission source. Moreover, changing the normal direction of the coil can provide multi-angle electromagnetic values. The angle between the coil and the x-axis, z-axis or y-axis and z-axis are $\alpha \in (0, \pi/2)$ and $\theta \in (0, \pi/2)$. The emission can be expressed by horizontal and vertical magnetic dipole sources. Based on the vector stack, the electromagnetic field underground in any position can be expressed as follows:

$$\begin{bmatrix} H_x^{VMD} & H_x^{HMD} \\ H_y^{VMD} & H_y^{HMD} \\ H_z^{VMD} & H_z^{HMD} \\ E_x^{VMD} & E_x^{HMD} \\ E_y^{VMD} & H_y^{HMD} \end{bmatrix} \begin{bmatrix} \sin\theta\cos\alpha \\ \cos\theta \end{bmatrix} = \begin{bmatrix} H'_x \\ H'_y \\ H'_z \\ E'_x \\ E'_y \end{bmatrix}, \tag{21}$$

$$\begin{bmatrix} H_x^{VMD} & H_x^{HMD} \\ H_y^{VMD} & H_y^{HMD} \\ H_z^{VMD} & H_z^{HMD} \\ E_x^{VMD} & E_x^{HMD} \\ E_y^{VMD} & H_y^{HMD} \end{bmatrix} \begin{bmatrix} \sin\theta\sin s\alpha \\ \cos\theta \end{bmatrix} = \begin{bmatrix} H'_x \\ H'_y \\ H'_z \\ E'_x \\ E'_y \end{bmatrix}, \tag{22}$$

where H' and E' represent the electromagnetic values in angles α and θ, respectively. The formula above can be used in mine TEM-forward modeling at any location.

C. 2.5-D DAMPED LEAST SQUARES INVERSION

Based on the forward formula, the damped least squares method is an optimal regularization method, which takes account of the computation time and convergence stability. Moreover, the iterative process of this method can invert the optimal parameters quantitatively and obtain an accurate inversion result. The damped least squares method is widely used in geophysical inverse problems and can be expressed as follows [18], [23]–[25]:

$$p_{k+1} = p_k - (R_k^T R_k + \alpha I)^{-1} R_k^T e_k, \tag{23}$$

where I, p_k, and R_k represent the unit matrix, the change of the model parameters, and the Jacobian matrix, respectively. α denotes the damping factor, which is used to control the convergence direction of p_k and avoid divergence during the iteration. e_k denotes the relative error of the magnetic field's vertical component, specifically expressed as

$$e_k = \frac{\hat{H}_z - H'_z(\rho_k)}{\hat{H}_z}, \tag{24}$$

where $\hat{H}_z$ represents the observed value, ρ_k represents the 1-D inversion results by the SA-PSO algorithm, and $H'_z(\rho_k)$ denotes the advanced calculation value of the model.

Using the difference quotient instead of the derivative to obtain the Jacobian matrix, the Jacobian matrix can be expressed as follows:

$$R_k = \frac{H'_z(\rho_k + \delta\rho) - H_z(\rho_k)}{\delta\rho_j}, \tag{25}$$

where $\delta\rho$ represents the step size, which is essential to the difference. A large $\delta\rho$ can increase the inversion result error, whereas a small $\delta\rho$ can make the operator matrix considerably small to produce an accurate inversion result. Normally, $\delta\rho = 0.001 \sim 0.01$.

The fitting result is evaluated using the root mean square error criterion:

$$\phi(\rho_k) = \frac{1}{ml}\sum_{j=1}^{l}\sum_{t=1}^{m} e(\rho_k)^2, \tag{26}$$

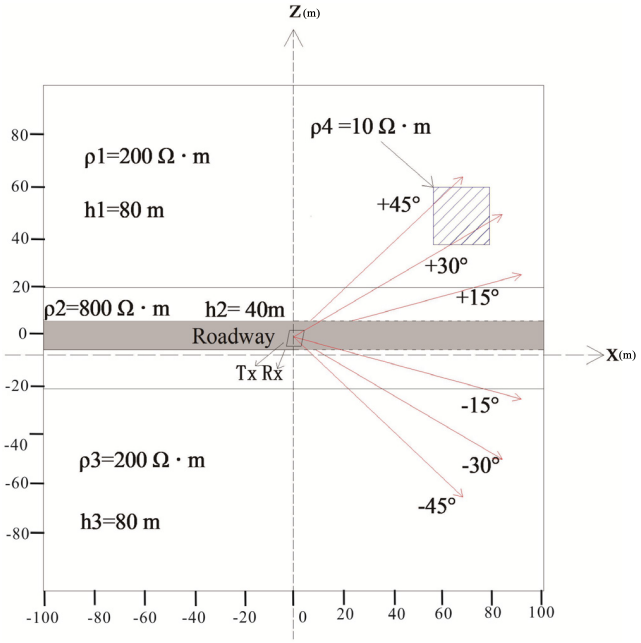

FIGURE 3. Diagram of multi-angle detection.

where ϕ represents the fitting function, m represents the sampling time, and l represents the number of detection directions.

The specific inversion process is as follows:

(1) Invert the observed electromagnetic field with any angle using the 1-D SA-PSO algorithm to obtain the initial inversion model $\rho_{i,j}$.

(2) Assign $\rho_{i,j}$ to the corresponding grid points with depth and direction. Then based on the features of the layer model, the 2.5-D inversion ρ_k can be obtained by interpolation.

(3) Apply ρ_k to the damped least squares algorithm as the initial model, then the new model ρ_{k+1} can be updated by formula (23). Quitting the process or using ρ_{k+1} to recalculate depends on whether the accuracy requirement of the relative error e_k is met.

D. SYNTHETIC SIMULATION

A three-layer geoelectric model is established as a simulation model, which locates in front of the heading face and contains a low-resistivity anomaly in the roof sandstone of the coal layer. Figure 3 shows that along the profile of y = 0, the abnormal body is designed as 20 m × 20 m in size with 10 Ω · m resistivity and is located 60 m in front of the heading face, with its lower boundary at 20 m above the roadway. The emission and receiving coil are set up in the model center (0, 0). The SA-PSO algorithm is used to invert the model with six advanced detection angles. The inversion results are shown in Figure 4.

The 1-D inversion results (Figure 4), which are basically consistent with the established model, are applied as an initial model to the 2.5-D damped least squares inversion. Taking the misfit error and computation time into account, we used the 10^{th} iteration results of inversion. The iterative fitting

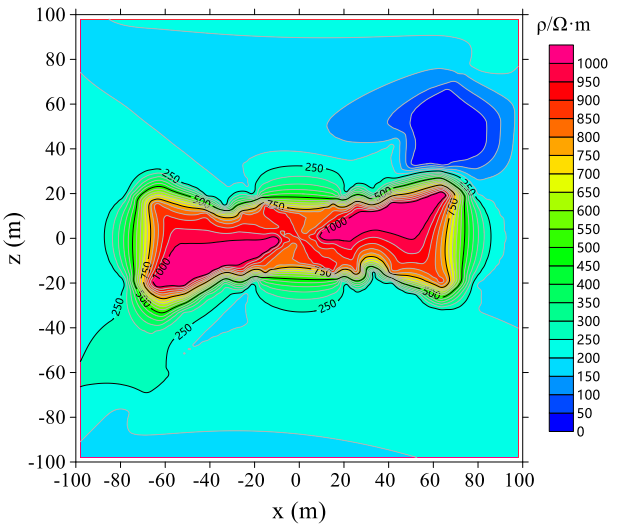

FIGURE 4. 1-D inversion results.

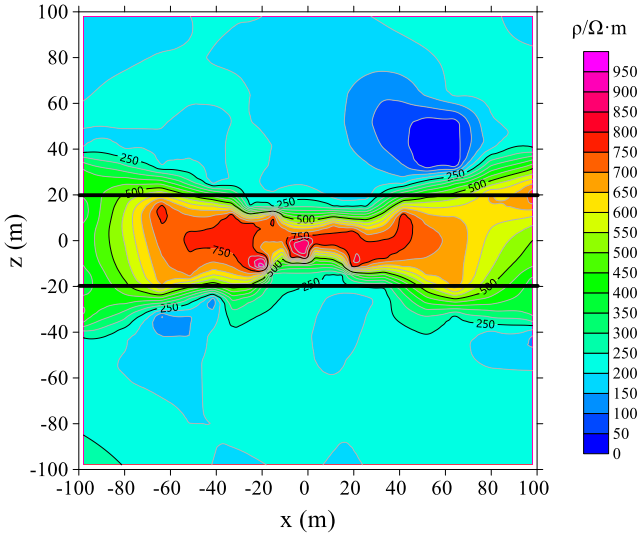

FIGURE 5. Inversion profile by 2.5-D method.

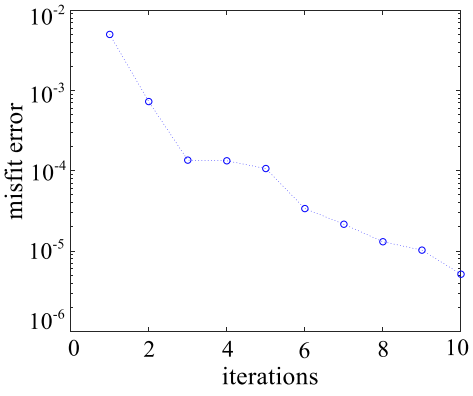

FIGURE 6. Error curve of iterations.

error curve is shown in Figure 6. The fitting error gradually decreases, from 5×10^{-3} to 5×10^{-6}, whereas the convergence is stable. Figure 5 shows the inverse resistivity profile with layered characteristic and resistivity basically coincides

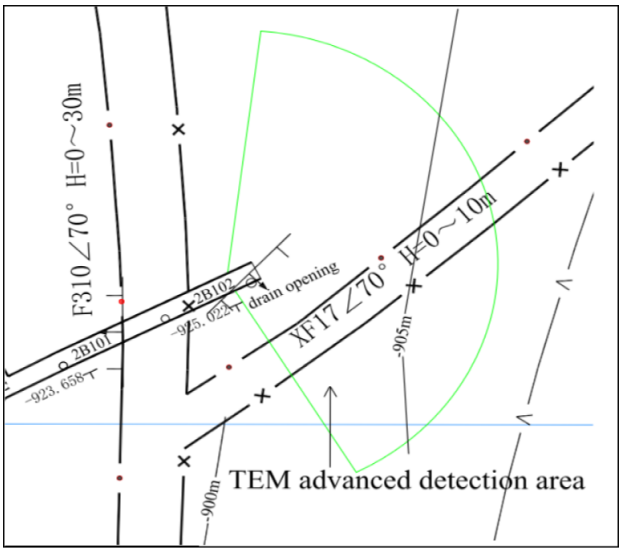

FIGURE 7. Planar graph of exploration area.

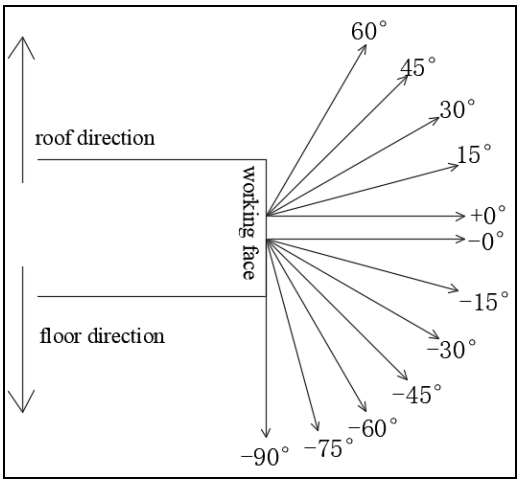

FIGURE 8. Diagram of advanced detection figure.

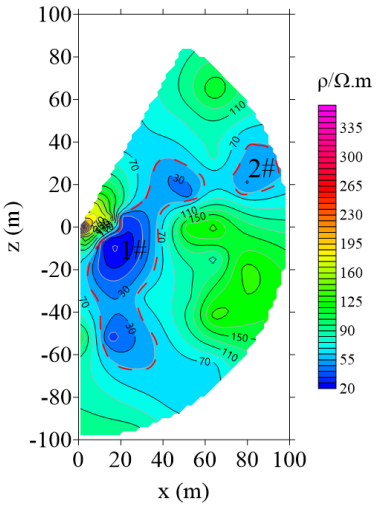

FIGURE 9. Field data resistivity profile 1-D inversion.

with the established model, and the low-resisivity anomalous body is relatively obvious. The 2.5-D inversion results of the resistivity values are higher than the theoretical values in the middle of the model because of the initial model of 1-D inversion results. Some inversion points in the first layer of the model are lower than the actual value because the initial data are insufficient, which result in the fitting error to not be changed at every point in the grid. Therefore, some points' parameters deviate from theactual values, although the fitting error decreases. Moreover, the mesh step near the boundary is bigger than others, which results in single anomaly values, thereby leading to a large anomaly area. Overall, the inverted resistivity profile has a good resolution and distinct layer structure, which is basically consistent with the established model. The location of the low-resistivity abnormality is accurate, and the resolution is evidently improved compared with 1-D inversion.

V. ENGINEERING APPLICATION EXAMPLE

We applied the method to the engineering of advanced TEM detection in Shandong Province, in the east of China to evaluate the 2.5-D inversion method for advanced detection mine TEM in full space. Previous geological information indicated the possible existence of two faults F310 and XF17 (Figure 7). Locating the two faults before roadway development was necessary. Thus, we could apply mine TEM to detect the distribution of water-rich and water-channel strata ahead of the heading face and near the water point. The TerraTEM system was used to collect multi-angle field data (Figure 8). The layer threshold values of resistivity and depth were calculated before performing 2.5-D inversion.

Figure 9 shows the inverted profile by 1-D SA-PSO. The point (0, 0) represents the mine advanced detection position, and the advanced detection area within X > 0. In Figure 9, the inverted resistivity mainly ranges within 0–400$\Omega \cdot m$, and two low-resistivity anomalies exist, with anomalous bodies 1 and 2 at approximately 50–100 $\Omega \cdot m$ and 20–50$\Omega \cdot m$, respectively.

The 2.5-D inversion method produces a different resistivity inversion profile using the 1-D inversion results as the initial model (Figure 10). The low-resistivity anomaly 2 in the 2.5-D inversion is more obvious and accurate within 20–50 $\Omega \cdot$ m compared with the 1-D inversion. However, anomaly 1 is not obvious around the shallow heading face because of the turn-off time effect. The inversion profile is spread on the structural exploration profile to reflect the electrical distribution characteristics of the anomaly area, which locates on the heading face. Figure 11 shows that the center of the low-resistivity anomaly corresponds well with the location of the limestone layer. We speculate that the low resistivity around the water point is a water-bearing fissure zone. The inversion results basically are consistent with the actual hydrogeological situation in the measured area based on drilling and roadway data.

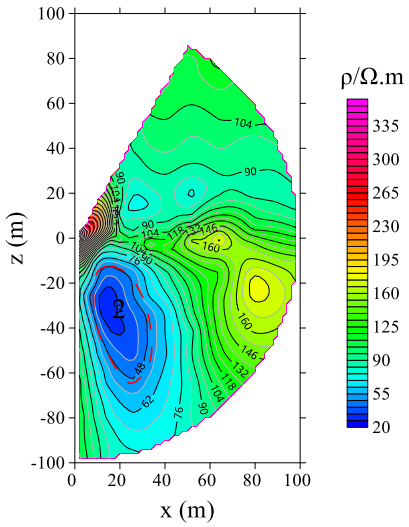

FIGURE 10. 2.5-D inversion resistivity profile for measured data.

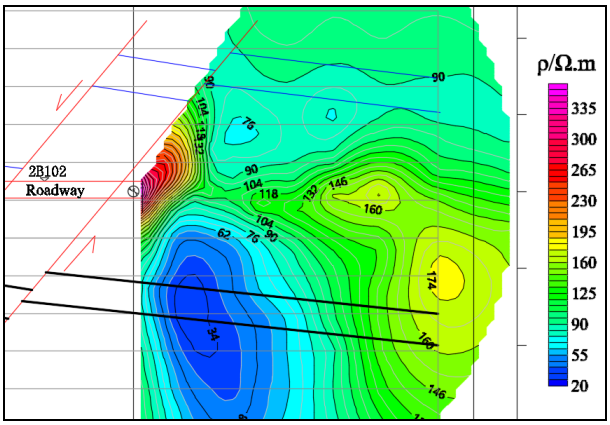

FIGURE 11. Overlap map of 2.5-D inversion profiles and structural exploration profiles.

VI. CONCLUSION

A 2.5-D inversion method for mine TEM-advanced detection is proposed in this paper. A vector synthesis method is used to initialize the electromagnetic values with multiple angles at the first step to process and explain the proposed method accurately. The SA-PSO inversion method can solve the issue of the traditional PSO method which always converges to local optimal values. The 2.5-D inversion can accelerate convergence speed by the 1-D inversion results of the SA-PSO method as the initial model. The damped least squares method is a typical inversion algorithm for obtaining stable results along the steepest descent direction. Thus, applying this method to the 2.5-D inversion can guarantee accuracy and resolution. Subsequently, we used a full-space advanced model simulation and case study to verify the method proposed in this paper. The inverted profiles are consistent with the theoretical model and the actual hydrogeology. In summary, this paper tested the effectiveness of the proposed 2.5-D inversion method in mine TEM detection with multiple angles. Moreover, the method used has a vital theoretical and practical ability to improve the accuracy and resolution of mine TEM in full space.

DECLARATION OF INTEREST

The authors declare no conflict of interests regarding the publication of this article.

REFERENCES

[1] J. Yu, R. Malekian, J. Chang, and B. Su, "Modeling of whole–space transient electromagnetic responses based on FDTD and its application in the mining industry," *IEEE Trans. Ind. Informat.*, vol. 13, no. 6, pp. 2974–2982, Dec. 2017.
[2] W.-Y. Chen, G. Q. Xue, Y. K. Muhammad, L. J. Gelius, N.-N. Zhou, H. Li, and H.-S. Zhong, "Application of short–offset TEM (SOTEM) technique in mapping water–enriched zones of coal stratum, an example from East China," *Pure Appl. Geophys.*, vol. 172, no. 6, pp. 1643–1651, Jun. 2015.
[3] J. Chang, J. Yu, and B. Su, "Numerical simulation and application of mine TEM detection in a hidden water-bearing coal mine collapse column," *J. Environ. Eng. Geophys.*, vol. 22, no. 3, pp. 223–234, Sep. 2017.
[4] J. L. Cheng, F. Li, and S. P. Peng, "Research progress and development direction on advanced detection in mine roadway working face using geophysical methods," *J. China Coal Soc.*, vol. 39, no. 8, pp. 1742–1750, 2014.
[5] G.-Q. Xue, C.-Y. Bai, S. Yan, S. Greenhalgh, M.-F. Li, and N.-N. Zhou, "Deep sounding TEM investigation method based on a modified fixed central-loop system," *J. Appl. Geophys.*, vol. 76, pp. 23–32, Jan. 2012.
[6] G. Q. Xue, J. L. Cheng, N. N. Zhou, W. Y. Chen, and H. Li, "Detection and monitoring of water-filled voids using transient electromagnetic method: A case study in Shanxi, China," *Environ. Earth Sci.*, vol. 70, no. 5, pp. 2263–2270, Nov. 2013.
[7] D. Chen, J. Cheng, and A. Wang, "Numerical simulation of drill-hole transient electromagnetic response in mine roadway whole space using integral equation method," *Chin. J. Geophys.*, vol. 61, no. 10, pp. 300–311, 2018.
[8] Z. Jiang, S. Liu, and R. Malekian, "Analysis of a whole–space transient electromagnetic field in 2.5-dimensional FDTD geoelectric modeling," *IEEE Access*, vol. 5, pp. 18707–18714, 2017.
[9] C. Jiu-Long, C. Ding, X. Guo-Qiang, Q. Hao, and Z. Xiang-Tong, "Synthetic aperture imaging in advanced detection of roadway using mine transient electromagnetic method," *Chin. J. Geophys.*, vol. 59, no. 2, pp. 190–198, Mar. 2016.
[10] G. Y. Chen, L. B. Du, and J. E. Jing, "2.5D inversion algorithm and parameters of marine controlled-source electromagnetic method," (in Chinese), *Prog. Geophys.*, vol. 31, no. 4, pp. 1796–1802, 2016.
[11] H. Wang and Y. Luo, "Algorithm of a 2.5-dimensional finite element mothed for transient electromagnetic with a central loop," *Chin. J. Geophys.*, vol. 46, no. 6, pp. 1227–1240, Nov. 2003.
[12] B. Xiong and Y.-Z. Luo, "Finite element modeling of 2.5-D FEM with block homogeneous conductivity," *Chin. J. Geophys.*, vol. 49, no. 2, pp. 515–525, Mar. 2006.
[13] R. Schaa and P. K. Fullagar, "Rapid, approximate 3D inversion of transient electromagnetic (TEM) data," in *Proc. SEG Tech. Program Expanded Abstr.*, Jan. 2010.
[14] G. Y. Chen, Z. Lei, and H. H. Jing, "Study on the application effect of 2.5 D marine inversion using the nonlinear conjugate gradient algorithm," *J. Ocean Technol.*, vol. 37, no. 2, pp. 13–18, 2018.
[15] M. Li, A. Abubakar, and T. M. Habashy, "Cross well electromagnetic interpretation using 2.5D model based inversion algorithm," in *Proc. SEG Tech. Program Expanded Abstr.*, Jan. 2009.
[16] G. Wilson, A. Raiche, and F. Sugeng, "2.5D inversion of airborne electromagnetic data," *Explor. Geophys.*, vol. 37, no. 4, pp. 363–371, Dec. 2006.
[17] C. Kirkegaard and E. Auken, "A parallel, scalable and memory efficient inversion code for very large-scale airborne electromagnetics surveys," *Geophys. Prospecting*, vol. 63, no. 2, pp. 495–507, Mar. 2015.
[18] W.-B. Li, Z.-F. Zeng, J. Li, X. Chen, K. Wang, and Z. Xia, "2.5D forward modeling and inversion of frequency-domain airborne electromagnetic data," *Appl. Geophys.*, vol. 13, no. 1, pp. 37–47, Mar. 2016.
[19] J. K. Qiang, K. F. Man, and J. B. Long, "2.5-D nonlinear conjugate gradient inversion of airborne transient electromagnetism in time domain," *Chin. J. Geophys.*, vol. 59, no. 12, pp. 4701–4709, 2016.

[20] U. C. Das, "Frequency-and time-domain electromagnetic responses of layered earth—A multiseparation, multisystem approach," *Geophysics*, vol. 60, no. 1, pp. 285–290, Jan. 1995.
[21] A. Godio and A. Santilano, "On the optimization of electromagnetic geophysical data: Application of the PSO algorithm," *J. Appl. Geophys.*, vol. 148, pp. 163–174, Jan. 2018.
[22] K. A. Dowsland and J. M. Thompson, Eds., "Handbook of natural computing," in *Annealing*. Leiden, The Netherlands: Leiden Univ., 2012, ch. 49.
[23] N. Ruan, D. Y. Gao, and Y. Jiao, "Canonical dual least square method for solving general nonlinear systems of quadratic equations," *Comput. Optim. Appl.*, vol. 47, no. 2, pp. 335–347, Oct. 2010.
[24] S. R. Buss, "Introduction to inverse kinematics with Jacobian transpose, pseudoinverse and damped least squares methods," *IEEE J. Robot. Autom.*, vol. 17, nos. 1–19, p. 16, Apr. 2004.
[25] H. Y. Yang, F. P. Li, S. E. Chen, J. H. Yue, F. S. Guo, X. Chen, and H. Zhang, "An inversion of transient electromagnetic data from a conical source," *Appl. Geophys.*, vol. 15, pp. 545–555, Sep. 2018.

JIULONG CHENG is working with the China University of Mining and Technology, Beijing, as a Professor. He has been engaging in the research of geophysical prospecting technology in coal mines. His main research direction is the application of seismic prospecting and electromagnetic prospecting in the fields of mining and engineering.

JUNJIE XUE received the master's degree in applied mathematics from the Liaoning University of Technology, Jinzhou, China, in 2019. He is currently pursuing the Ph.D. degree with the China University of Mining and Technology, Beijing. His research interest includes electromagnetic inversion.

JIN ZHOU received the master's degree from the China University of Mining and Technology, Beijing, in 2018. He is currently an Assistant Engineer with China Railway Eryuan Engineering Group Company Ltd. His research interest is engineering geophysics.

YI DONG is currently pursuing the Ph.D. degree with the China University of Mining and Technology, Beijing. His research interest includes geophysical forward and inversion.

LAIFU WEN is currently working as a Lecturer with the Hebei University of Engineering. He has engaged in engineering geophysics, geophysical forward and inversion, and geophysical joint inversion.